Dynamics of Field-Induced Ordering in Magnetic Colloids Studied by New Time-Resolved Small-Angle Neutron-Scattering techniques

A. Wiedenmann,[1*] U. Keiderling,[1] K. Habicht,[1] M. Russina,[1] and R. Gähler[2]

[1] Hahn-Meitner-Institut, Structure Research, Glienicker Str. 100, D-14109 Berlin, Germany

[2] Institut Laue-Langevin, BP. 85X, F-38042 Grenoble Cedex, France

[*] corresponding author: e-mail: wiedenmann@hmi.de

The reversal of magnetic moments of nanoparticles in concentrated Co-ferrofluids was monitored in an oscillating magnetic field by new time-resolved stroboscopic small-angle neutron-scattering techniques. Time resolution in the µs range was achieved by using a pulsed beam technique, TISANE, while in continuous mode resolution was limited by the wavelength spread to about 1ms. The frequency dependence of anisotropic scattering patterns has been modeled using Langevin dynamics. The dynamics follows a two step mechanism: Field induced ordering is governed by fast Brownian rotation of nanoparticles with a characteristic time of about 160 µs. Magnetic relaxation of locally ordered domains of about 100 nm in size takes place within a few seconds by Brownian rotation or by Néel type rotation of magnetic moments.

PACS numbers: 75.50.Tt, 61.12.Ex, 47.65.Cb, 75.10.-b

Dynamical studies of nanosized inhomogeneities by means of small-angle neutron scattering (SANS) usually are limited to slow processes where the system remains in a quasi-steady state during data acquisition time. A breakthrough to time resolution of microsecond range was achieved by new SANS techniques, allowing the dynamics of fast ordering processes in Co-ferrofluids to be analysed.

SANS studies using polarized neutrons have shown that in concentrated Co ferrofluids interactions between superparamagnetic particle moments are induced by an external magnetic field, giving rise to an unusual pseudocrystalline hexagonal ordering of the nanosized magnetic particles [1]. Locally ordered domains of typically 100 nm in size coexist with flexible dipolar chains [1,2]. In previous time-dependent SANS experiments, the relaxation of local ordering has been studied when the saturation magnetic field was switched off [3]. Magnetic correlations between nanoparticles were found to decay exponentially within a characteristic time order of 1-5 s. The onset of the local ordering, however, was too fast to be observed by this direct mode. In order to study the dynamics of reversal and reordering of the particle moments, a periodic sine-wave modulation of the magnetic field was applied to the sample and combined with new time-resolved SANS techniques. Here we present the setup and advantages of two techniques for investigation of oscillating processes by means of SANS: a direct stroboscopic mode using a continuous neutron flux is compared to a pulsed time-resolved technique TISANE [4] based on the FOTOF technique [5].

A magnetic field generating coil with a ferrite core was operated with a high-stability frequency generator and power amplifier. Periodic sine-wave modulations of the vertical magnetic field up to amplitudes of B_{Max} = 26 mT and frequencies between ν_s = 50 Hz and

3000 Hz could be applied to the sample placed in the homogenous part of the magnetic field. The reversibility of the reordering process in the dynamic mode has been checked by comparing the stroboscopic SANS results with those measured in the same coil device with a static magnetic field of the same amplitude. The sample was the same concentrated Co-ferrofluid (MFT3) as used in [2,3], consisting of 6 vol. % Co-nanoparticles of R_c = 4.4 nm radius coated with a shell of oleylsarcosin as surfactants with a thickness of D_s=1.9 nm and dispersed in a viscous oil L9.

Stroboscopic experiments have been performed on the SANS instrument V4 at BENSC, Berlin, using a continuous neutron beam with a wavelength band of $\Delta\lambda/\lambda = 0.11$ at $\lambda = 0.605$ nm. The area detector was placed at a distance of L_2 = 4 m from the sample. Data acquisition was triggered by the frequency generator and operated in list mode, i.e. every single scattered neutron was registered together with its time stamp. Data have been grouped in histograms of 128 x 128 pixels of 0.5 x 0.5 cm^2 for position and n = 100 time channels of widths $\Delta t = (n\nu_s)^{-1}$. The neutron time-of-flight is given by

$$t_{TOF}[ms] = \lambda[nm] \times L_2[m] \times 2.52778 \qquad (1)$$

leading to a delay of the detector response with respect to the magnetic field of $t_{TOF}/\Delta t$ channels. Because of the phase shift $\varphi \approx -\pi/2$ between the ac voltage producing the trigger signal and the induced magnetic field, the time channels corresponding to zero field depend on the frequency according to $n_t(B=0) = (t_{TOF}/\Delta t) \pm \varphi(100/2\pi)$. The Q range 0.2 nm^{-1} < Q < 1.2 $nm^{-1}$and resolution of the order of $\Delta Q/Q < 0.1$ allowed to resolve the characteristic correlation peaks at Q_1 = 0.39 nm^{-1} and Q_3 = 0.29 nm^{-1} [3].

In the TISANE technique (Fig. 1), a pulsed polychromatic beam is produced by a chopper at a distance L_1 from the sample. The chopper frequency ν_e is locked-in with the oscillation frequency ν_s of the magnetic field and the data acquisition frequency of the detector ν_d. All three frequencies are different and must satisfy the conditions

$$\nu_d = \nu_s - \nu_e \text{ for } \nu_e L_1 = (\nu_s - \nu_e) L_2 . \qquad (2)$$

Figure 1 shows that all neutrons from different chopper pulses elastically scattered by the sample in a given oscillation state are collected in the same time frame of the detector, irrespective of their wavelengths. Considerable gains in intensity and time resolution are obtained when a large frame overlap (i.e. long distances) and high repetition rates can be achieved. The TISANE principle has been realized at the time-of-flight instrument NEAT at BENSC, using a fast single chopper with variable frequencies up to ν_e = 666 Hz at L_1 = 13 m which according to Eq. (2) allowed a maximum frequency of the ac field of ν_s = 2800 Hz. Scattered neutrons have been collected in the area detector at L_2 = 4 m in histograms of 32 x 32 pixels of 3 x 3cm^2 and 128 time channels. Using the polychromatic beam with 0.2 nm < λ < 2 nm a Q range between 0.1 and 4 nm^{-1} was covered. The Q resolution was relaxed to the order of $\Delta Q/Q \approx 0.35$.

Results from the continuous stroboscopic technique are presented first. At low frequencies a periodic response to the oscillating magnetic field was clearly observed in the 2D scattering patterns. For the time channels corresponding to B_{Max} = ±20 mT the scattering is strongly anisotropic as shown in Fig. 2(a) for ν_s = 100 Hz while for B = 0 the patterns are almost isotropic. The SANS intensities averaged over a width of 20° in sectors at an angle α = 30° and 90° between **Q** and **B** are plotted in Fig. 2(b) as a function of Q together with the corresponding curves for the static case. In the static case at 20 mT, sixfold symmetry of the

pattern is visible by the peaks at $Q_1(\alpha = 30°\text{and } 90°) = 0.39$ nm^{-1} corresponding to the in-plane reciprocal lattice vectors, while the shoulder observed at $Q_3 = 0.29$ nm^{-1} corresponds to the inter-plane vector. Segments of chains are spontaneously formed by dipolar interactions between particle moments giving rise to a characteristic Q^{-1} dependence of the intensities observed in both sectors at low Q [2]. In the static case, these fragments are partly aligned along the external field and randomly distributed at zero field, while in the dynamic experiment the alignment of the magnetic moments and the local hexagonal arrangement of the nanoparticles are only partly established. Intensities have been integrated in angle sectors $\alpha = 0°$, 30°, and 90° over the Q ranges shown in Fig. 2(b) and denoted by Q_A, Q_B, and Q_C. The time dependence of the intensities $I(Q_{i,\alpha})$ is shown in Fig. 2(c) for $\nu_s = 100$ Hz for i = A, B, C and α = 0°, 30°, and 90° and in Fig 3(a) for different frequencies at $Q_B(0°)$ and $Q_B(90°)$, respectively. The periodicity of the response is twice that of the magnetic field and the peak positions agree perfectly with the values expected from Eq. (1). With increasing frequencies the intensity oscillations decrease in amplitude and fade away above about $\nu_s = 600$ Hz. While the intensity levels in Fig. 2(c) are nearly identical for both time channels corresponding to B = 0, $n_t(B = 0) = 35.8$ and 85.8, the amplitudes are slightly higher in the second half period at B = 20 mT ($n_t = 11$) than in the first one at B = -20 mT ($n_t = 61$), which can be best seen at α = 0°. This asymmetry results from a residual static (guide) field of 1-2 mT oriented downwards which superimposes on the applied oscillating field. This effect is quantitatively taken into account in the treatment below.

The SANS intensity is given by

$$I(\mathbf{Q},\alpha,B,T) = f_e\int\{(F_M{}^2L^2(x)\sin^2\alpha + F_N{}^2)S(\mathbf{Q},\alpha) + F_M{}^2[2L(x)/x - \sin^2\alpha(L^2(x) - 1 + 3L(x)/x)]\}D(\Delta\lambda,\nu_s)d\Delta\lambda + (1-f_e)U(\mathbf{Q},\alpha,\nu_s) \quad (3)$$

The term in braces was derived for single-domain particles in equilibrium [6,7]. F_N and F_M are the nuclear and magnetic form factors of the particles defined by $F_{N,M}(QR) = \int dr^3 \Delta\eta_{N,M} \exp(i\mathbf{Qr})$ with the corresponding scattering contrasts $\Delta\eta_{N,M} = \eta_{N,M} - \eta_{matrix}$. $S(\mathbf{Q},\alpha)$ is an effective anisotropic structure factor which accounts for interparticle interactions [1,2]. The dependence on the magnetic field enters in Eq. (3) via the Langevin function L(x), where $x = V_c m_0 B(t)/(k_B T)$. V_c is the core volume and m_0 is the spontaneous magnetisation of Co. As long as all particle moments follow the oscillating magnetic field, the SANS pattern should be described by Eq. (3) using

$$B(t) = B_{\max} \sin(2\pi\nu_s t) + B_{st}, \qquad (4)$$

where B_{st} is the correction term for the residual static field. $U(\mathbf{Q},\alpha,\nu_s)$ represents a time-independent scattering contribution. The term in braces has to be convoluted with $D(\Delta\lambda,\nu_s)$ which accounts for the smearing of the oscillations due to a spread of t_{TOF} times. For the present case of a triangular wavelength distribution of $\Delta\lambda/\lambda = 0.11$ from the velocity selector, $\lambda = 0.605$ nm, and $L_2 = 4$ m, the relative time spread of the signal increases linearly with the frequency according to $\Delta t_R/T_s = \Delta\lambda t_{TOF}\nu_s$ from 6% at 100Hz to 36% at 600 Hz [bars in Fig. 3(a)]. The damping factors $D(\Delta\lambda,\nu_s)$ have been evaluated to decrease from 1.0 in the static case to 0.93 at 100 Hz, 0.77 at 200 Hz, 0.63 at 300 Hz to 0.11 at 600 Hz. Excellent agreement of all data was obtained by the model function of Eq. (3) as shown by the solid lines in Fig. 2(c). and Fig. 3(a) when a unique set of parameters was for all frequencies. In particular, the decrease of the amplitudes and the increase of the apparent gap between the intensities $I(Q_{B,0})$ and $I(Q_{B,90})$ at $n_t(B = 0)$ result solely from the wavelength smearing. For the sectors Q_C, the structure factors $S(Q,\alpha) = 1$ corresponding to single particle scattering while $S(Q_A)$ and $S(Q_B)$ differ significantly from unity due to inter-plane and intra-chain (Q_A) and in-plane (Q_B) correlations [2,3]. The total intensity range shown in Fig. 3(a) corresponds to $I(Q_{B,0}) = 12.4$ and $I(Q_{B,90}) = 23.3$ as measured in a static magnetic field of B = 20 mT. While the decrease of the

amplitudes between 100 and 600 Hz is explained by the damping factors $D(\Delta\lambda,\nu_s)$ alone, the amplitude observed at 100 Hz is only about half of the static case and much lower than expected from the factor $D(\Delta\lambda,\nu_s = 100) = 0.93$. Instead, it clearly indicates that at 100 Hz only a fraction f_e of the particle moments are still freely oscillating [Eq. (3)]. The rest does not follow the external field but remains frozen more or less randomly, leading to the time-independent term $(1- f_e)U(Q,\alpha,\nu)$ in Eq. (3). In fact, from a simultaneous fit of all data it turned out that $U(Q,\alpha,\nu)$ is independent of α and ν. It corresponds closely to the intensity as measured in the static mode at B = 0 [dashed lines in Fig. 3(a)] and which is expected for a random orientation of magnetic particle moments in zero magnetic field, where $L(x)\rightarrow 0$, $L(x)/x\rightarrow 1/3$ and hence $U(Q) = F^2_N S(Q) + 2/3F^2_M(Q)$ [6,7]. The fraction f_e of superparamagnetic moments which follows the field reversal was found to be of the order of 55% and nearly constant between 100Hz and 600Hz. At higher frequencies no reliable information on the dynamics can be derived from the continuous stroboscopic technique due to large damping factors $D(\Delta\lambda,\nu_s)$.

In the TISANE technique, however, the time resolution at the detector is given by

$$\Delta t_R^{\,2} = (\Delta t_e L_2 / L_1)^2 + [\Delta t_s (L_1 + L_2)/L_1]^2 + (\Delta t_d^{\,2}) \quad (5)$$

which is dominated by the chopper pulse lengths of 50-500 μs given by $\Delta t_e = 0.035/\nu_e$ for the present chopper slit and frequency range, compared to $\Delta t_s \approx \Delta t_d/2 \approx 1.5$ μs. Since time resolution Δt_e, sample cycle time T_s and detection duty cycle T_d scale inversely with the chopper frequency, the damping of the TISANE signal is independent of the oscillation frequency and much weaker than in the continuous SANS mode, i.e. $\Delta t_R/T_S \approx 3.5\%$ [bars in Fig.3(b)]. The 2D scattering patterns in the pulsed TISANE experiment were found to oscillate from nearly isotropic at $n_t(B = 0)$ to strongly anisotropic at $n_t(\pm B_{max})$. Intensities

$I(Q_{\alpha=0})$ and $I(Q_{\alpha=90})$ integrated over full angle sectors of 30° width, corresponding to an average value of $Q_B = 0.4 \pm 0.3$ nm^{-1} are presented in Fig. 3(b) for several frequencies and different field amplitudes. This shows impressively how the pulsed TISANE technique largely extends the frequency range of the continuous mode. Up to about 1300 Hz, the intensities oscillated again with a frequency twice of the B-field while at 1420 Hz and 2800 Hz no intensity modulation remained. The signal shows no asymmetry of the amplitudes since no static magnetic (guide) field was present at the NEAT instrument. The frequency dependence of the intensity was analysed as before in terms of Eq. (3) using $B_{st} = 0$ and a frequency independent damping $D(\Delta\lambda,\nu_s)$ which corresponds to the actual value of $\Delta t_R/T_S \approx$ 3.5%. The amplitudes of the oscillations measured at 300 Hz with $B_{max} = 16$ mT and 600 Hz with $B_{max} = 26$ mT, respectively, solely differ due to different values of the Langevin parameters $L(B_{max} = 16\ mT) = 0.53$ and $L(B_{max} = 26mT) = 0.69$, respectively [Eq. (3)]. The simultaneous fit of the oscillations measured between 300Hz and 1099Hz at two values of B_{max} according to Eq. (3) confirmed that the amount of freely oscillating moments f_e really decreases from 55% at 300 Hz and 50% at 600Hz to 30% at 1099 Hz and drops to 0 at 1424 Hz. It has to be emphasized that the time independent 2D pattern at 1424 Hz was fully isotropic and no gap appeared between $I(Q_{\alpha=0})$ and $I(Q_{\alpha=90})$ showing the random moment orientation in the fully frozen state. The difference to SANS pattern at 600Hz [Fig. 3(a)] is obvious, where the apparent anisotropic behavior resulted from time averaging of oscillating patterns.

The data combined from the continuous and TISANE techniques indicate a relaxation process which reflects the polydispersity of ordered domains, and is basically in agreement with ac susceptibility measurements [8]. For about 40% of the particles, moment rotation is blocked already below 100 Hz while between 600 and 1300 Hz the remaining particle moments

continuously freeze out in a random orientation. The second step around $\nu = (2\pi\tau_B)^{-1} \approx$ 1000-1300 Hz corresponds closely to the characteristic time τ_B = 160 μs expected for Brownian rotational diffusion of individual core-shell particles of radius $R_p = R_c + D_s$ = 6.4 nm and a viscosity η = 0.2 Pas for the liquid L9, according to $\tau_B = 4\pi\eta R_p^{\,3}/(k_B T)$. The field-induced ordering process must be governed by the fast particle rotation causing the magnetic moments to align along the direction of the magnetic field. Then the moments get stuck into locally ordered domains of about 100 nm in size. Magnetic relaxation takes place either by Brownian rotation of the whole domain or by rotation of magnetic moment inside the particle against the anisotropy energy barrier K_A according to the Néel mechanism given by $\tau_N = f_o \exp(K_A V_c^{\,3}/k_B T)$. The characteristic time of both mechanisms is expected to be 1-50 s, which corresponds closely to the values observed previously when the field was switched off allowing for full relaxation into equilibrium [3]. This slow relaxation of large ordered domains is at the origin of low frequency step. The incomplete relaxation gives rise to frozen random orientation of particle moments observed in an oscillating magnetic field. The sticking of particles must be induced by the strong dipolar interactions energy given by

$$E_{dd} = (\mu_0/4\pi) m_0^{\,2} V_c^{\,2}/\sigma^3 \qquad (6)$$

which amounts to $E_{dd}/(k_B T) = 3$ for a pair in closest contact $\sigma = 2(R_c + D_s)$. Molecular dynamics studies predicted the observed hexagonal ordering [9] which might be favored by attractive depletion interactions via nonmagnetic micelles and interactions from fluctuating parallel dipolar chains.

In summary, the new time-resolved stroboscopic SANS techniques present a real breakthrough for dynamical studies of nanoscaled inhomogeneities. The limitation of the continuous technique arises from the wavelength smearing Δλ/λ. While the Q resolution was

better in the stroboscopic SANS technique, a clear superiority of TISANE occurs concerning the time resolution. In the present case of the reordering dynamics in ferrofluids, the observed threshold frequency around 1300 Hz is a real physical quantity since this value is still far below the instrumental time resolution and corresponds to Brownian rotation of core-shell particles. The pulsed TISANE technique gives access to a submillisecond time scale which has never been accessible to neutron scattering up to now. This technique allows the dynamics of field-induced processes to be studied while complementary studies on magnetic colloids by dynamic susceptibility measurements [10], photon correlation spectroscopy with visible light (PCS) or x rays (XPCS) [11], and forced Rayleigh scattering [12] probe natural fluctuations in zero fields. Whenever the scattering system responds to a periodic perturbating field in a measurable way, this modulation technique can close - at least part of - the time gap between Mössbauer and inelastic neutron scattering techniques (10^{-6}-10^{-12} s) [13] and static measurements.

We thank K. Thillosen for setting up the solenoid device and acknowledge the financial support of the German research foundation (DFG) project Wi 1151/3.

Figure captions:

FIG. 1. (Color online) Distance-time diagram for the TISANE mode. A wide velocity band of neutrons emerges from successive chopper openings (E) causing frame overlap at the sample (S). Neutrons from different chopper pulses which probe the same oscillation state are observed at the same time channel at the detector (D), if Eq. (2) is satisfied.

FIG. 2. (Color online) SANS intensities (a) in the 2D pattern and (b) after radial averaging in the static and dynamic (ν_s = 100 Hz, B_{max} = ±20 mT) modes. In-plane (Q_1) and interplane (Q_3) vectors are marked. (c) Time dependence at Q_A, Q_B, and Q_C. Solid lines: fits to Eq. (3).

FIG. 3. (Color online) Frequency dependence of scattering intensities. Bars indicate the experimental resolution. (a) Stroboscopic SANS mode at Q_B. (b) TISANE mode. Symbols: 0° (closed), 90° (open). Solid lines: fits to Eq. (3). Dashed lines: static SANS mode B = 0.

Figure 1:

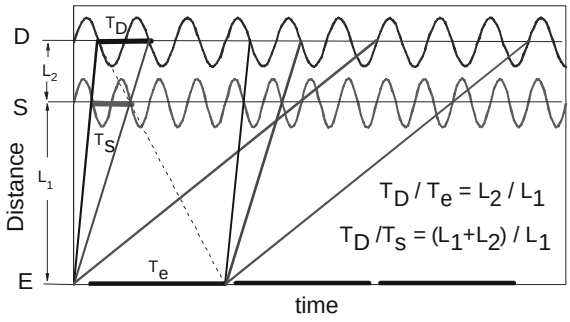

Figure 2:

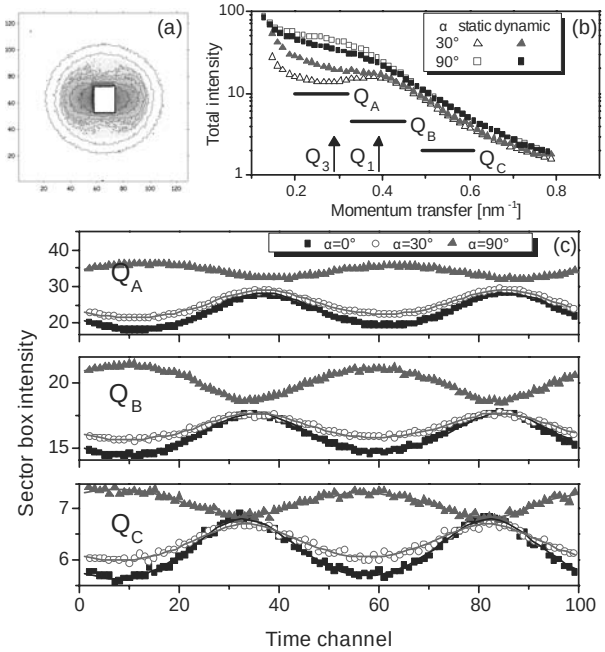

Figure 3:

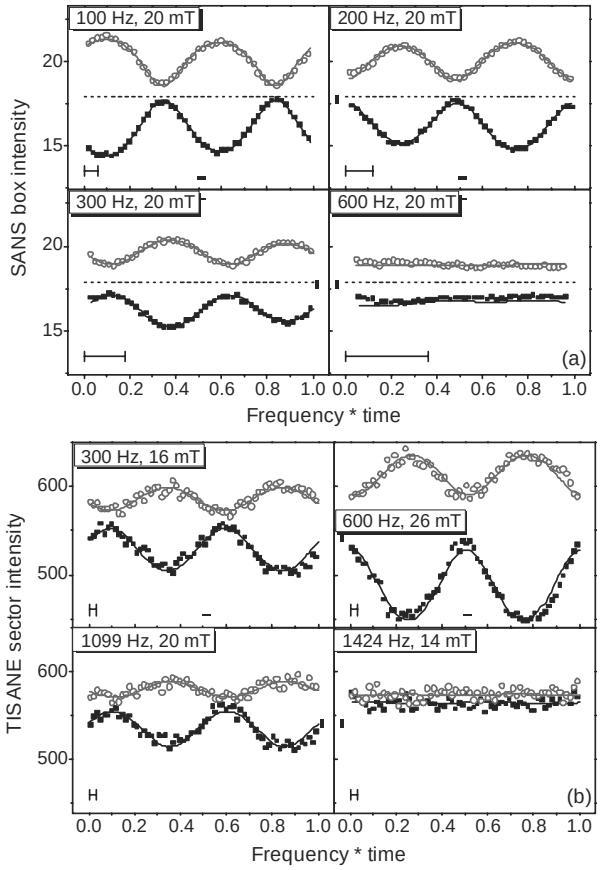
100 Hz, 20 mT
200 Hz, 20 mT
300 Hz, 20 mT
600 Hz, 20 mT
SANS box intensity
20
15
(a)
0.0 0.2 0.4 0.6 0.8 1.0
Frequency * time
300 Hz, 16 mT
600 Hz, 26 mT
1099 Hz, 20 mT
1424 Hz, 14 mT
TISANE sector intensity
600
500
H
(b)
Frequency * time

[1] A. Wiedenmann, A. Hoell, M. Kammel, and P. Boesecke, Phys. Rev. E **68**, 031203 (2003).

[2] A. Wiedenmann and A. Heinemann, J. Magn. Mater. **289**, 58-61 (2005).

[3] A. Wiedenmann, U. Keiderling, R. May, and C. Dewhurst, Physica B (Amsterdam) to be published.

[4] R. Gähler and R. Golub, ILL SC **99-1**, 73 (1999).

[5] R. Gähler and R. Golub, Z. Phys. B Cond. Mat. **56**, 5-12 (1984).

[6] R. Pynn, J.B. Hayter, and S.W. Charles, PRL **51**, 710-713 (1983).

[7] J. Kohlbrecher, A. Wiedenmann, and H. Wollenberger, Z. Phys. B **104**, 1-4 (1997).

[8] A. Wiedenmann, U. Keiderling, and B.H. Erné (to be published).

[9] S. Hess, edited by S.A. Safran and N.A. Clark, (Wiley, New York, 1987), pp. 631-642.

[10] B.H. Erné, K. Butter, B.W.M. Kuipers, and G.J. Vroege, Langmuir **19**, 8218-8225 (2003).

[11] J. Lal, D. Abernathy, L. Auvray, O. Diat, and G. Grübel, Eur. Phys. J. **E4**, 263-271 (2001).

[12] J.C. Bacri, A. Cebers, A. Bourdon, G. Demouchy, B.M. Heegaard, and R. Perzynski, Phys. Rev. Lett. **74**, 5032 (1995).

[13] M.F. Hansen, F. Bodker, S. Morup, K. Lefmann, K.N. Clausen, and P.A. Lindgard, Phys. Rev. Lett. **79**, 4910-4913 (1997).